Spatial and Temporal Propagation of Scatterometer Winds

Davit Harutyunyan

March 3, 2011

1 Goal of the project

Ocean models are generally forced by synthetic (global) NWP model wind fields. It has however been shown that these fields lack mesoscale wind structures on scales below 500 km, i.e., on the ocean eddy scale. Also, compared to wind observations, NWP model wind fields have persistent wind direction biases and lack response to SST gradients or air-sea temperature difference.

Based on Kolmogorov turbulence theory it is well known that the wind in the boundary layer has a kinetic energy spectrum with wave number power slope of $-5/3$ in mesoscales. It is a very important property and preservation of this property in dynamical models can significantly improve ocean forcing.

The scatterometers nowadays provide a very accurate measurement of wind over the ocean and the retrieved winds contain the mesoscale structure consistent with the Kolmogorov theory. The scatterometer winds are available over the ocean only at a specific time and at a specific location. The goal of this project is to propagate the physically correct scatterometer winds both in time and space and provide a uniform wind forcing over the ocean.

For the spatial and temporal propagation of the scatterometer winds we use a simplified dynamical model of Boussinesq type which is forced by ECMWF pressure field. The scatterometer winds are incorporated into the model by using a simple nudging approach.

2 Boundary layer model

Over the tropics and near the tropics the boundary layer can be considered as well-mixed, where the velocity is considered to be constant in height, see [22, 17, 18, 20, 10]. In this case, by using the hydrostatic assumption, the Reynolds averaging and averaging over the height of the mixed boundary layer, one can write the momentum and continuity equations in the following form

$$\frac{\partial u}{\partial t}+u\frac{\partial u}{\partial x}+v\frac{\partial u}{\partial y}-fv+g'\frac{\partial(h+h_s)}{\partial x}=-\frac{1}{\rho_0}\frac{\partial p}{\partial x}-\frac{C_d|\mathbf{u}_|u}{h}+w_e\frac{u_g-u}{h}, \quad (1a)$$

$$\frac{\partial v}{\partial t}+u\frac{\partial v}{\partial x}+v\frac{\partial v}{\partial y}+fu+g'\frac{\partial(h+h_s)}{\partial y}=-\frac{1}{\rho_0}\frac{\partial p}{\partial y}-\frac{C_d|\mathbf{u}_|v}{h}+w_e\frac{v_g-v}{h}, \quad (1b)$$

$$\frac{\partial h}{\partial t}+\frac{\partial hu}{\partial x}+\frac{\partial hv}{\partial y}=w_e, \quad (1c)$$

where $\mathbf{u}=(u,v)$ is the velocity, h is the mixed-layer height and h_s is the topography (over ocean it is ignored, i.e. $h_s=0$ for the res of this report), g' is the reduced gravity, C_d is the surface drag coefficient and w_e denotes the entrainment velocity. The wind on top of the mixed layer is denoted by (u_g,v_g) and the mean sea level pressure is denoted by p.

2.1 In spherical coordinates

If one has to consider the model over a large region, then the earth sphericity has also to be considered. To write the system (1) in the spherical coordinates let us first recall couple of relations between the spherical and the Cartesian coordinate systems.

If we denote the longitude and the latitude by λ and φ, respectively, then we have the following relation

$$\mathrm{d}x=R\cos\phi\,\mathrm{d}\lambda, \quad \mathrm{d}y=R\mathrm{d}\varphi, \quad (2)$$

where R is the radius of the earth.

After substitution of (2) in (1) we obtain the equations of the motion in the spher-

ical coordinates:

$$\frac{\mathrm{d}u}{\mathrm{d}t} - fv + \frac{g'}{R\cos\varphi}\frac{\partial h}{\partial \lambda} = -\frac{1}{\rho_0 R\cos\varphi}\frac{\partial p}{\partial \lambda} - \frac{C_d|\mathbf{u}|u}{h} + w_e\frac{u_g - u}{h}, \tag{3a}$$

$$\frac{\mathrm{d}v}{\mathrm{d}t} + fu + \frac{g'}{R}\frac{\partial h}{\partial \varphi} = -\frac{1}{\rho_0 R}\frac{\partial p}{\partial \varphi} - \frac{C_d|\mathbf{u}|v}{h} + w_e\frac{v_g - v}{h}, \tag{3b}$$

$$\frac{\mathrm{d}h}{\mathrm{d}t} + \frac{h}{R\cos\varphi}\frac{\partial u}{\partial \lambda} + \frac{h}{R}\frac{\partial v}{\partial \varphi} = w_e, \tag{3c}$$

where the total derivative in the spherical coordinates is

$$\frac{\mathrm{d}}{\mathrm{d}t} = \frac{\partial}{\partial t} + \frac{u}{R\cos\varphi}\frac{\partial}{\partial x} + \frac{v}{R}\frac{\partial}{\partial y}.$$

2.2 In conservative form

From the numerical discretization point of view it is desirable to write the system (3) into an equivalent conservative form [1]

$$\frac{\partial u}{\partial t} - \frac{1}{\cos\varphi}\left(-\frac{1}{R}\frac{\partial E}{\partial \lambda} - \frac{1}{R}\frac{\partial (g'h)}{\partial \lambda} + Z(hv\cos\varphi)\right) - \frac{h}{R\cos\varphi}\frac{\partial g'}{\partial \lambda} = \tag{4a}$$

$$-\frac{1}{\rho_0}\frac{\partial p}{\partial x} - \frac{C_d|\mathbf{u}|u}{h} + w_e\frac{u_g - u}{h},$$

$$\frac{\partial v}{\partial t} + \frac{1}{\cos\varphi}\left(\frac{\partial E}{\partial \varphi} + \frac{\partial (g'h)}{\partial \varphi} + Z(hu)\right) - \frac{h}{R}\frac{\partial g'}{\partial \varphi} = \tag{4b}$$

$$-\frac{1}{\rho_0}\frac{\partial p}{\partial y} - \frac{C_d|\mathbf{u}|v}{h} + w_e\frac{v_g - v}{h},$$

$$\frac{\partial h}{\partial t} + \frac{1}{R\cos\varphi}\left(\frac{\partial (hu)}{\partial \lambda} + \frac{\partial (hv\cos\varphi)}{\partial \varphi}\right) = w_e, \tag{4c}$$

where

$$E = \frac{1}{2}(u^2 + v^2),\ Z = \frac{f+\xi}{h},\ \xi = \frac{\partial v}{\partial x} - \frac{\partial u}{\partial y} - \text{vorticity}.$$

This set of equations are discretized with a finite difference method on a C-grid. In the absence of the external forces the resulted discrete system is conservative. For details about the discretization on Arakawa C-grid we refer to [1].

3 Boundary conditions

Because we consider the model on a limited area, then proper lateral boundary conditions are required. There are different types of boundary conditions for limited area models, however it is not very straightforward to point out the best boundary conditions applicable for all problems.

I have basically considered Orlanski type open boundary conditions and its variations, see for example [15, 3, 7, 16, 12]. For hyperbolic type of problems Orlanski proposed to use the following condition on the boundary

$$\frac{\partial \phi}{\partial t} + c\frac{\partial \phi}{\partial \mathbf{n}} = 0, \tag{5}$$

where c is the phase velocity of the wave (still to be determined), $\mathbf{n}$ is the normal to the boundary and ϕ is any predictive variable. For example, if we consider a limited area with lateral boundaries along latitudes and longitudes, then on the west and south boundaries the boundary condition (5) is modified into the following form

$$\frac{\partial \phi}{\partial t} - c\frac{\partial \phi}{\partial x} = 0 \text{ and } \frac{\partial \phi}{\partial t} - c\frac{\partial \phi}{\partial y} = 0,$$

respectively. Similarly, on the east and north side it would be

$$\frac{\partial \phi}{\partial t} + c\frac{\partial \phi}{\partial x} = 0 \text{ and } \frac{\partial \phi}{\partial t} + c\frac{\partial \phi}{\partial y} = 0,$$

respectively.

The phase velocity c has to be determined numerically and there are different ways to compute c from (5).

For my problem I have tried the Orlanski boundary condition and also some of its variations [15, 3, 7, 16, 12]. However I have to admit that there was no best open boundary condition applicable everywhere. In some cases I had to change between one condition to the other to find out the better condition. In general these type of boundary conditions work, but in some small part on the boundaries the numerical wave speed is not determined correctly and it leads to some wrong oscillations close to the boundary.

It is pointed out in [13] that using (5) may result in unbalance between the boundary layer height and the velocity, and this could lead to spurious strong localized

velocity gradients at the boundaries. It is suggested in [13] to add to the right hand side of (5) some of additional terms (pressure gradient force, the surface drag) to make more robust boundary condition. I have also tried this approach and the results have been improved a bit, but there were still problems at the boundaries.

4 Pressure gradient force

The wind in our model is basically forced by the pressure gradient. In our case pressure (the mean sea level pressure) is not a predictive parameter, I rather consider it as an external input.

If one considers a relatively small region then the geostrophic approximation can be applied. In this case the pressure gradient force is replaced with constant geostrophic wind, see for example [5, 8, 13, 23].

In my opinion we can not use the geostrophic approximation over larger domains and for a longer simulation period. Therefore I decided to use the mean sea level pressure (hereafter pressure) from ECMWF.

To use the ECMWF pressure in my model I have done the following steps: first I retrieved the pressure from ECMWF using source of *Operational archive, Atmospheric model, Forecast*. This provides pressure on a user pre-defined resolution in every three hour. Because in the model during the time integration the pressure gradient force (PGF) needs to be evaluated at every time step, then I applied a simple linear interpolation in time. However I have to stress out that this approach is not that popular and there are very few papers where this kind of pressure interpolation is used, see for example [4, 19].

5 Physical parametrization

To complete the description of our dynamical model it remains to discuss parametrization of surface drag coefficient (C_d) and the entrainment velocity (w_e) in (3).

There is an established theory for the parametrization of the surface drag and there are also many ways to compute C_d. But for the parametrization of w_e there is no unified theory and it is hard to say which parametrization approach is the best.

5.1 Drag coefficient parametrization

For simplicity we consider the drag coefficient in neutral conditions. In this case the stratification of the atmosphere is ignored and the resulting formulas become simpler. For our experiments we follow the formulation presented in [11].

In a neutral condition the wind speed u_z in the surface layer at a given height z relates to the surface roughness length z_0 by the following formula

$$u_z = \frac{u_*}{\kappa} \ln(\frac{z}{z_0}), \tag{6}$$

where u_* is the friction velocity and $\kappa = 0.41$ is the von Karman constant.

Over the sea and oceans the surface roughness length is determined by the Charnock relation

$$z_0 = C_{ch}\frac{u_*^2}{g} + 0.11\frac{\nu}{u_*}, \tag{7}$$

where $C_{ch} = 0.018$ is the Charnock parameter and $\nu = 1.5 \cdot 10^{-5}\,\mathrm{m^2 s^{-1}}$ is the kinematic viscosity of air.

And finally the drag coefficient is determined as

$$C_d = \frac{\kappa^2}{\ln^2(\frac{z}{z_0})}. \tag{8}$$

The surface roughness length z_0 is computed from the coupled nonlinear system of equations (6) and (7). Because in our model equations we are interested in determining the 10 meter wind, then it is also logical to consider in (6) the reference length $z = 10$ meter.

The system (6) and (7) is a nonlinear set of equations for u_* and z_0 which can be solved with Newton Raphson method. It means that in every time step we have to apply the nonlinear solver at each grid point in the computational domain. This can be very costly and will consume to much time to determine the drag coefficient.

In the code called UWPBL [2] which is used in [17, 18] a very simple iterative approached is used to determine the roughness length.

Let us define an error tolerance ε for computation of the friction velocity and the maximum iterations to be I_0. Then the following algorithm is used to determine the drag coefficient:

Algorithm 1 Computation of the drag coefficient C_d, the friction velocity u_* and the roughness length z_0

SET $z = 10$ m and we assume u_{10} is given from the model
Set (for example) $\varepsilon = 10^{-8}$ and $I_0 = 50$
Set $u_*^{error} = 10$ and $I_{count} = 0$
Initialize $u_* = 0.35$
while $u_*^{error} < \varepsilon$ and $I_{count} < I_0$ **do**
    $z_0 = C_{ch}\frac{u_*^2}{g} + 0.11\frac{\nu}{u_*}$,
    $u_*^{new} = \kappa\frac{u_{10}}{\ln(\frac{z}{z_0})}$
    $u_*^{error} = |u_*^{new} - u_*|$
    $u_* := u_*^{new}$
    $I_{count} = I_{count} + 1$
end while
$C_d = \frac{\kappa^2}{\ln^2(\frac{z}{z_0})}$

5.2 Entrainment parametrization

There are many ways to parametrize the entrainment velocity, see for example [].

In my experiments I used the parametrization suggested by [23]

$$w_e = \frac{C_F}{C_T}\left(\frac{2.5}{C_F}\right)^{1/3} u_* \tag{9}$$

where u_* is the friction velocity, $C_F = 0.2$ and $C_T = 1.5$.

6 Newtonian nudging

The Newtonian nudging is a very simple, easy to implement assimilation method, which can be used to nudge the model simulation towards the available observa-

tions. For our problem we use the nudging algorithm described in [14] with the scatterometer wind observations.

The basic idea is the following. For any given predictive variable α (u or v) its corresponding equation at any given point $\mathbf{x}_i$ is modified into the following form

$$\frac{\partial \alpha(\mathbf{x},t)}{\partial t} = F(\alpha,\mathbf{x},t) + G\frac{\sum_{j=1}^{N}(W_j(\mathbf{x}-\mathbf{x}_j,t-t_j))^2(\alpha_j-\alpha_i(\mathbf{x}_j,t))}{\sum_{j=1}^{N}W_j(\mathbf{x}-\mathbf{x}_j,t-t_j)}, \qquad (10)$$

where F represents all the physical process. The second term is the nudging contribution, where the summation is performed over the all observations. **It is important to note that the nudging terms are evaluated at the observation points.**

The weighting functions W_j as defined in [14] are given by

$$W_j = w_{xy}(D_j)\cdot w_\sigma(\sigma-\sigma_j)\cdot w_t(t-t_j),$$

where w_σ, w_{xy} and w_t are the vertical, the horizontal and the time weights, respectively. Note that in our case $w_\sigma = 1$, because we consider only two dimensional problem.

The spatial weight w_{xy} is a Cressman-type weighting function which depends on the distance between the observation point and the grid point and is defined as

$$w_{xy} = \frac{1-D_j^2/R^2}{1+D_j^2/R^2}, \qquad \text{if} \quad D_j \le R,$$
$$w_{xy} = 0, \qquad \text{if} \quad D_j > R,$$

where R is a predefined radius of influence and D_j is the distance between the observation point and the grid point.

Here is a list of references where the scatterometer winds are used in a dynamical model with nudging method [6, 21, 9].

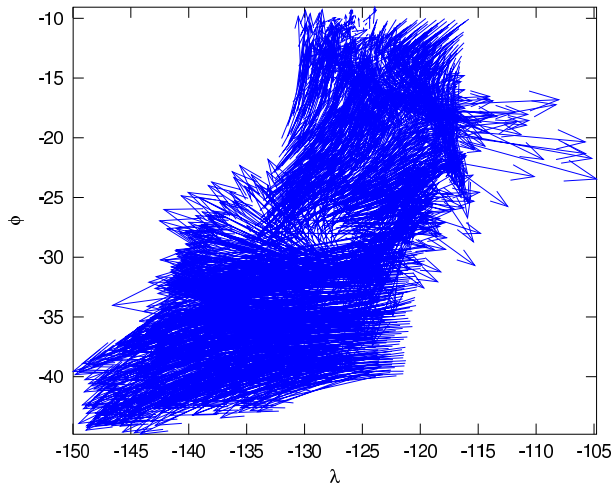

Figure 1: The simulation domain, where the scatterometer winds are available.

7 Simulation results

The model (3) is discretized on a uniform Arakawa A lat-lon grid on the area $[-140^\circ, -110^\circ] \times [-40^\circ, -10^\circ]$ with spatial resolution 0.2° is both directions. The model is initialized on 01-11-2010 at 0 UTC with ECMWF wind and is run for 9 hour. For this test case we use ASCAT 25 km resolution wind product which is available for our example during 2 UTC – 2:30 UTC.

The simulation domain and the scatterometer winds are given in Figure 1.

First we compare the results running the model by using the scatterometer wind as a nudging term with the results of the model without any scatterometer wind. Because the scatterometer winds are available between 2 UTC – 2:30 UTC in Figure 2 we show the kinetic energy spectrum averaged between 1:30 UTC – 4 UTC. The results show that by using the scatterometer winds the model in mesoscales produces (specially for the v component) more kinetic energy than without the scatterometer data. However the results are not yet encouraging enough, because from the theoretical point of view we expect to have -5/3 spectrum, which is clearly not a case at mesoscales.

To check how long can the model carry the inserted scatterometer mesoscale energy in time in Figure 3 we present results by running the model with the scat-

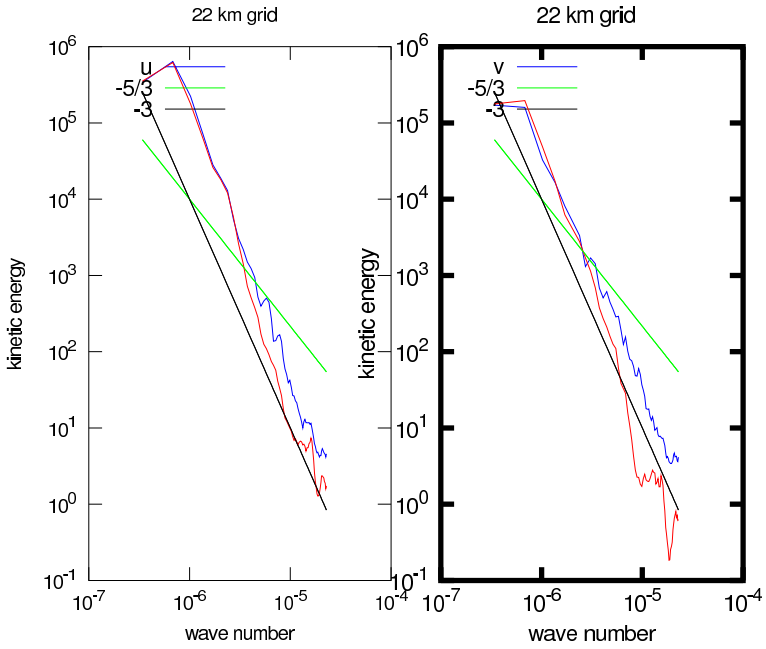

Figure 2: Comparison of the kinetic energy spectrum by using scatterometer winds for nudging (blue line) and the model run without nudging (red line). The spectrum is averaged between 1 UTC and 4 UTC.

terometer winds. The blue line shows the spectrum averaged between 1 UTC – 4 UTC and the red line corresponds to the results averaged 5 UTC – 8 UTC. Because the scatterometer data are available at around 2 UTC then we expect to have more kinetic energy between 1 UTC – 4 UTC. Indeed, as we can see at mesoscales around 1 UTC – 4 UTC (blue line) the model produces more energy than between 5 UTC – 8 UTC. But also we note while we progress in time the energy is not dissipated to much, which implies that the current model does not dissipate energy quickly.

8 Discussions

I have considered assimilation of the scatterometer winds using well-mixed boundary layer model (3). The model is discretized on an Arakawa-A grid, i.e. the

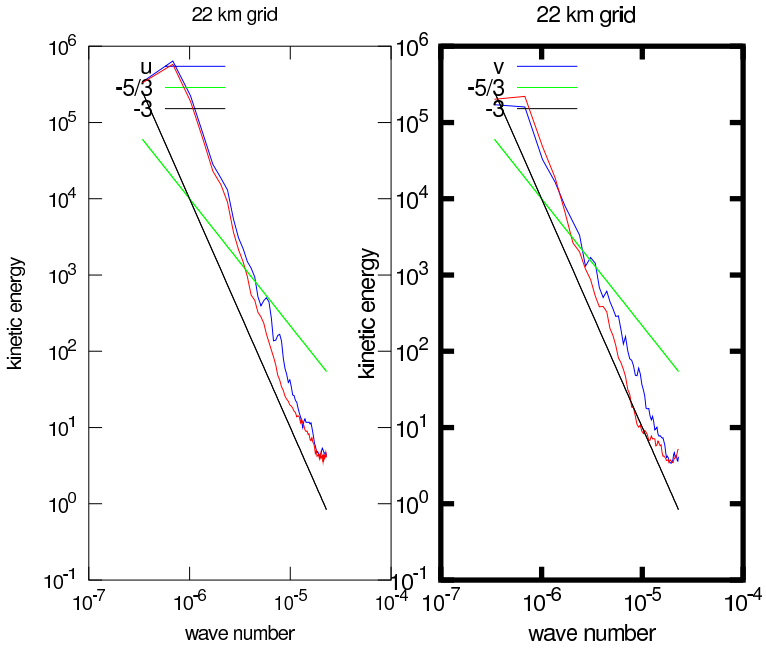

Figure 3: Comparison of the kinetic energy spectrum by using scatterometer winds for nudging. The spectrum averaged between 1 UTC – 4 UTC blue line, 5 UTC – 8 UTC red line.

variables are considered on the same grid point. It was observed that by using the scatterometer winds the kinetic energy spectrum of the assimilated wind has more energy in mesoscales (down to 20 km) as compared to the wind spectrum obtained without assimilation. However the slope of the kinetic energy spectrum is not consistent with the theoretical data, which predicts -5/3 slope.

References

[1] www.ecmwf.int/newsevents/training/rcourse_notes/NUMERICAL_METHODS/HORIZONTAL_DISCRETIZATION/Horizontal_discretization5.html.

[2] Uwpbl 4.1. http://pbl.atmos.washington.edu/Uwpbl30/home.html.

[3] A. L. Camerlengo and J. J. O'Brien. Open boundary conditions in rotating fluids. *J. Comput. Phys*, 1979.

[4] L. Carrre and F. Lyard. Modeling the barotropic response of the global ocean to atmospheric wind and pressure forcing - comparisons with observations. *GEOPHYSICAL RESEARCH LETTERS*, 2003.

[5] L. W. Eddington, J. J. O'Brien, and D. W. Stuart. Numerical simulation of topographically forced mesoscale variability in a well-mixed marine layer. *Monthly Weather Review*, 120, 1992.

[6] G. Grell, J. Dudhia, and D. Stauffer. A Description of the Fifth-Generation Penn State/NCAR Mesoscale Model (MM5). Technical report, 1994.

[7] Y.-J. Han, K. Ueyoshi, and J. W. Deardorff. Numerical study of terrain-induced mesoscale motions in a mixed layer. *J. Atmos. Sci.*, 39:2464–2476, 1982.

[8] Y.-J. Han, K. Ueyoshi, and J. W. Deardorff. Numerical study of terrain-induced mesoscale motions in a mixed layer. *Journal of Atmospheric Sciences*, 39, 1982.

[9] M. Mandal, U. C. Mohanty, and A. K. Das. Impact of satellite derived wind in mesoscale simulation of Orissa super cyclone. *Indian Journal of Marine Sciences (IJMS)*, 2006.

[10] M. McGauley and C. Zhang. Large-scale characteristics of the atmospheric boundary layer in the eastern pacific cold tongueitcz region. *J. Climate*, 2004.

[11] M. J. Miller, A. C. M. Beljaars, and T. N. Palmer. The sensitivity of the ecmwf model to the parameterization of evaporation from the tropical oceans. *Journal of Climate*, 1991.

[12] M. J. Miller and A. J. Thorpe. Radiation conditions for the lateral boundaries of limited-area numerical models. *Quarterly Journal of Royal Meteorological Society*, 1981.

[13] P. H. R. nad J. W. DEARDORFF. A numerical simulation of an atmospheric vortex street. *Tellus*, 1982.

[14] J. W. Nielsen-Gammon, R. T. McNider, W. M. Angevine, A. B. White, and K. Knupp. Mesoscale model performance with assimilation of wind profiler data: Sensitivity to assimilation parameters and network configuration. *Journal of geophysical research*, 112(D09119), 2007.

[15] I. Orlanski. A simple boundary condition for unbounded hyperbolic flows. *Journal of Computational Physics*, 1976.

[16] E. D. Palma and R. P. Matano. On the implementation of passive open boundary conditions for a general circulation model: The barotropic mode. *JOURNAL OF GEOPHYSICAL RESEARCH*, 1998.

[17] J. Patoux, R. C. Foster, and R. A. Brown. Global pressure fields from scatterometer winds. *Journal of applied meteorology*, 42:813–826, 2003.

[18] J. Patoux, R. C. Foster, and R. A. Brown. An evaluation of scatterometer-derived oceanic surface pressure fields. *Journal of Applied Meteorology and Climatology*, 47(3):835–852, 2008.

[19] R. M. Ponte, D. A. Salstein, and R. D. Rosen. Sea level response to pressure forcing in a barotropic numerical model. *Journal of Physical Oceanography*, 1991.

[20] D. J. Raymond, C. S. Bretherton, and J. Molinari. Dynamics of the intertropical convergence zone of the east pacific. *Journal of the Atmospheric Sciences*, 2005.

[21] D. R. Stauffer and N. L. Seaman. Use of Four-Dimensional Data Assimilation in a Limited-Area Mesoscale Model. Part i: Experiments with Synoptic-Scale Data. *Mon. Wea. Rev*, 1989.

[22] B. Stevens, J. Duan, J. C. McWilliams, M. Mnnich, and J. D. Neelin. Entrainment, Rayleigh friction, and boundary layer winds over the tropical pacific. *Journal of Climate*, 15(1):30–44, 2002.

[23] J. M. Wilczak and J. W. Glendening. Observations and mixed-layer modeling of a terrain-induced mesoscale gyre: The denver cyclone. *Monthly Weather Review*, 116, 1988.